Research Article

Dominant role of deglaciation in Late Pleistocene–Early Holocene sediment aggradation in the Upper Chenab valley, NW Himalaya

Saptarshi Dey[a]* [ORCID], Naveen Chauhan[b], Milan Kumar Mahala[b], Pritha Chakravarti[a], Anushka Vashistha[a], Vikrant Jain[a] and Jyotiranjan S. Ray[b,c]

[a]Indian Institute of Technology Gandhinagar, Gandhinagar, Gujarat - 382055, India; [b]Physical Research Laboratory Ahmedabad, Gujarat - 380009, India and [c]National Centre for Earth Science Studies, Thiruvananthapuram, Kerala - 695011, India.

Abstract

Sediment transfer from the interiors of the Himalaya is complex because the archives are influenced by both glacial and monsoonal cycles. To deconvolve the coupling of glacial and monsoonal effects on sediment transfer processes, we investigate the Late Pleistocene–Holocene sediment archive in the Upper Chenab valley. Optically stimulated luminescence (OSL) ages from the archive indicate major aggradation during ca. 20–10 ka. Isotopic fingerprinting using Sr-Nd isotopes in silt fractions together with clast counts in boulder-pebble fractions indicate a decreasing Higher Himalayan sediment flux in the archive with time. Decreasing clast size, increasing clast roundness, increasing matrix to clast ratio, and dominance of the Higher Himalayan sourcing unequivocally suggest strong glacial influence during the initial stages of the archive formation. This evidence also agrees with the existing retreat ages of glaciers in the Upper Chenab valley. Results of our study also show that the upper parts of the archive contain significant fluvial sediment contribution from the Lesser Himalaya, which suggests an active role of the stronger Indian Summer Monsoon (ISM) in the region during the Early Holocene. The apparent decrease in sediment supply from the Higher Himalayan sources could have been due to longer source-to-sink transport in the Early Holocene and/or increased hillslope flux from Lesser Himalayan sources.

Keywords: Sediment provenance, Isotopic source fingerprinting, OSL dating, Last glacial maximum, Indian Summer Monsoon, Himalaya

(Received 10 August 2021; accepted 20 September 2022)

INTRODUCTION

Tectonics and climate are the two main forcing agents that control erosion and sediment delivery from mountains to basins (e.g., Strecker et al., 2007; Clift, 2017; Adams et al., 2020). Although these two controlling factors could be coupled (e.g., Whipple, 2009; Godard et al., 2014), most studies link million-year time-scale sediment fluxes to tectonic perturbations (e.g., Vannay et al., 2004; Mandal et al., 2021), while millennial-scale variations in sediment transfer processes in the Himalaya are often attributed to climatic perturbations (e.g., Owen et al., 2002; Gibling et al., 2005; Bookhagen et al., 2006; Dey et al., 2016). Variations in climatic strength depend on 1–10 ka monsoon cycles and 50–100 ka glacial-interglacial cycles that influence river discharge and sediment flux (e.g., Goodbred and Kuehl, 2000; Bookhagen et al., 2005a, 2006; Clift et al., 2008; Bookhagen and Strecker, 2012; Scherler et al., 2015; Tofelde et al., 2017; Dey et al., 2021). The balance between discharge and sediment flux determines whether the drainage system will aggrade or degrade (Lane, 1955). When discharge is high, due to either strong monsoon or rapid deglaciation, the sediment flux is generally higher than

average (e.g., Dey et al., 2022). In a recently published study from the southern Himalayan front, we have shown that sediment flux during a strong climatic forcing was five times higher than average (Dey et al., 2022). Contrary to findings from the Himalayas, the 1999 Chi-Chi Earthquake in Taiwan (Dadson et al., 2004) and the 2008 Wenchuan Earthquake in China (Wang et al., 2017) triggered higher sediment yield, highlighting the role of seismic events in rapid mass transfer. Mountain belts, which host recurrent seismic events of medium to high magnitude, are therefore susceptible for seismically triggered mass transfers, even on shorter timescales.

Although millennial-scale sediment transfer processes are generally linked to variations in climatic forcing, studies from the Himalaya suggest contrasting responses from catchments during monsoon strengthening in the Late Pleistocene to Early Holocene. Most of the catchments in the low-elevation sectors of the Himalaya, which are devoid of large glaciers, have recorded valley aggradation during the Early Holocene strong Indian Summer Monsoon (ISM) phase (e.g., Bookhagen et al., 2006; Srivastava et al., 2008; Dey et al., 2016, 2021). There also have been reports of degradation of the transiently stored valley-fill sediments during the same strong ISM phase (e.g., Singh et al., 2001; Suresh et al., 2007; Ray and Srivastava, 2010; Kapannusch et al., 2020). On the other hand, in high-elevation glaciated landscapes, sediment transfer is associated with deglaciation episodes (e.g., Owen et al., 2002; Dortch et al., 2009; Joussain et al., 2016).

*Corresponding author email address: saptarshi.dey@iitgn.ac.in

Decoding the paleo-climatological information from hinterland sediment archives, which lie in the climate transition zone, is difficult because those sediment archives are affected by both monsoonal and glacial cycles. Attributing the sediment transfer processes to either monsoonal or glacial cycles becomes even more challenging when these two cycles overlap. Only a handful of studies have attempted to address this problem (e.g., Barnard et al., 2004; Scherler et al., 2015; Dutta et al., 2018; Chahal et al., 2019; Kapannusch et al., 2020). In a study from the glacially influenced upper Yamuna valley, Kapannusch et al. (2020) proposed that Late Pleistocene aggradation in the valley was driven mainly by reduced discharge, whereas higher Late Pleistocene erosion rates had a minor effect. On the contrary, Chahal et al. (2019) and Dutta et al. (2018) linked aggradation with higher sediment flux during strong monsoon phases and/or, deglaciation.

Global climate trends since 30 ka show a high degree of covariance between monsoonal and glacial fluctuations. Figure 1 demonstrates simulated changes in monsoon pressure index (ΔM%) in the Indian Ocean, simulated changes in precipitation (P%) in south Asia (after Dortch et al., 2009), and variations in northern hemisphere solar insolation (ΔS%) (after Prell and Kutzbach, 1987). Therefore, sediment archives that trap sediments from this time window are complex and need thorough investigations to deconvolve the glacial and monsoonal influences on sediment transfer. Currently, understanding about the role of glacial processes on the evolution of fluvial valleys in the Himalaya is at nascent stage.

To achieve the above, we investigated the Late Pleistocene–Holocene sediment archive near the Padder town in the upper Chenab valley in the interiors of the western Himalaya. We combined detailed field observations, valley morphology, sedimentology, sediment chronology, and isotope source fingerprinting to explore how sediment archives can record evidence of glacial retreat and monsoon intensification or any seismic influence. Our study also highlights the response of different lithotectonic domains to climate change in the Himalaya.

GEOLOGICAL BACKGROUND

The study area chosen for this work, Padder town and surroundings, is situated along the southeastern margin of the Kishtwar tectonic window in the interior of Kashmir Himalaya. Located at an elevation of ~1770–1800 m above mean sea level (amsl), the area is drained by the Chenab River and its northern tributary, the Padder River (Fig. 2). From this point onwards, we shall use
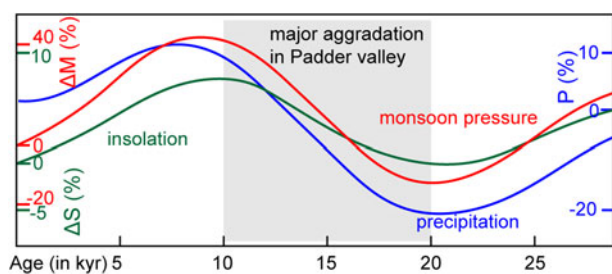
the term 'Padder valley' to refer to the study area. The Kishtwar Window exposes the Lesser Himalayan duplex, which is undergoing rapid exhumation at a rate of ~3.0–3.6 mm/yr for the last few million years (Gavillot et al., 2018). The eastern part of the window exposes quartzites of the Rampur Formation, intrusive granites, and highly sheared low- to medium-grade schists associated with the Main Central Thrust (MCT) shear zone (Fig. 2). In the hanging wall of the MCT, garnet- and staurolite-bearing Higher Himalayan crystalline rocks and farther upstream, the medium– high grade Higher Himalayan metasediments, known as the Haimantas, are exposed. The known exhumation rates from the Higher Himalaya are much lower than those of the Kishtwar Window (0.3–0.4 mm/y; Gavillot et al., 2018). The Chenab River, which originates in the Lahaul-Spiti region of the northern Himachal Pradesh, traverses ~350 km before reaching the Padder valley (Fig. 3a). The upstream reaches of the Chenab River and the southern flank of the Zanskar Range, which lie within the Higher Himalaya, are dominated by glaciers at present. During the last glacial maximum (LGM), the glacial extent was much greater, with most of the Higher Himalaya covered with ice (e.g., Kapannusch et al., 2020). In contrast, the Lesser Himalayan domain is sparsely populated by glaciers at present. Previous studies suggest that the upper Chenab valley has been subjected to glacial advancement and retreat across centennial to millennial timescales (Kulkarni et al., 2007; Eugster et al., 2016). Eugster et al. (2016) constrained the advancement of the Chenab valley glacier using [10]Be exposure ages from glacially polished Higher Himalayan bedrock (Fig. 3b). They reported glacial advancement down to ~2450 m above msl during the last glacial maximum (LGM), which remains as one of the lowest (w.r.t. elevation) known Himalayan glaciers during the LGM. The study area and surroundings receive 0.8–1.1 m/y rainfall (Bookhagen and Burbank, 2006). There is no record of historical seismicity in the nearby regions in the upstream, nor any records of significant earthquakes (Mw>3.5) in the last few decades (International Seismological Centre, 2021; Supplementary Figure S1). However, based on the evidence of last few decades or few centuries, we cannot comment on the seismic situation that prevailed during the formation of the archive.

METHODS

Field findings: Sediment log, clast count, valley morphology

The Padder valley records a ~90–95 m thick aggraded sediment sequence (Fig. 4a). The valley is filled with sediments of varying grain size, ranging from boulders to silt. Based on lithology and stratigraphy (and chronology) we divided the entire sediment archive of the valley into five sub-packages, from Qp1–Qp5. Each of the sub-packages shows an overall fining-upward sequence. In the lower parts of the archive (Qp1 and Qp2), we observed angular to sub-angular boulders at the bottom, followed by gravels in the middle, and sandy silt at the top. In the middle (Qp3), we observed sub-rounded pebbles at the base and silt at the top. The matrix content in Qp3 is higher than Qp1–Qp2, with smaller grainsize. In the upper part of the archive, in Qp4, we observed sub-rounded to well-rounded pebbles at the base and sand at the top. The pebbles show imbrications and clearly bear a fluvial signature. The sand bodies are often isolated and coarse grained. In Qp5, the clasts at the base are leucogranites, and are highly angular and disoriented. Qp5 is topped by a thick layer of silt.

Figure 1. Global climate trends since 30 ka demonstrated by simulated changes in monsoon pressure index (ΔM%) in Indian Ocean, simulated changes in precipitation (P%) in south Asia (after Dortch et al., 2009) and variations in northern hemisphere solar insolation (ΔS%) (after Prell and Kutzbach, 1987). These regional/global trends indicate overlap of glacial and monsoonal cycles in Late Pleistocene–Holocene time period.
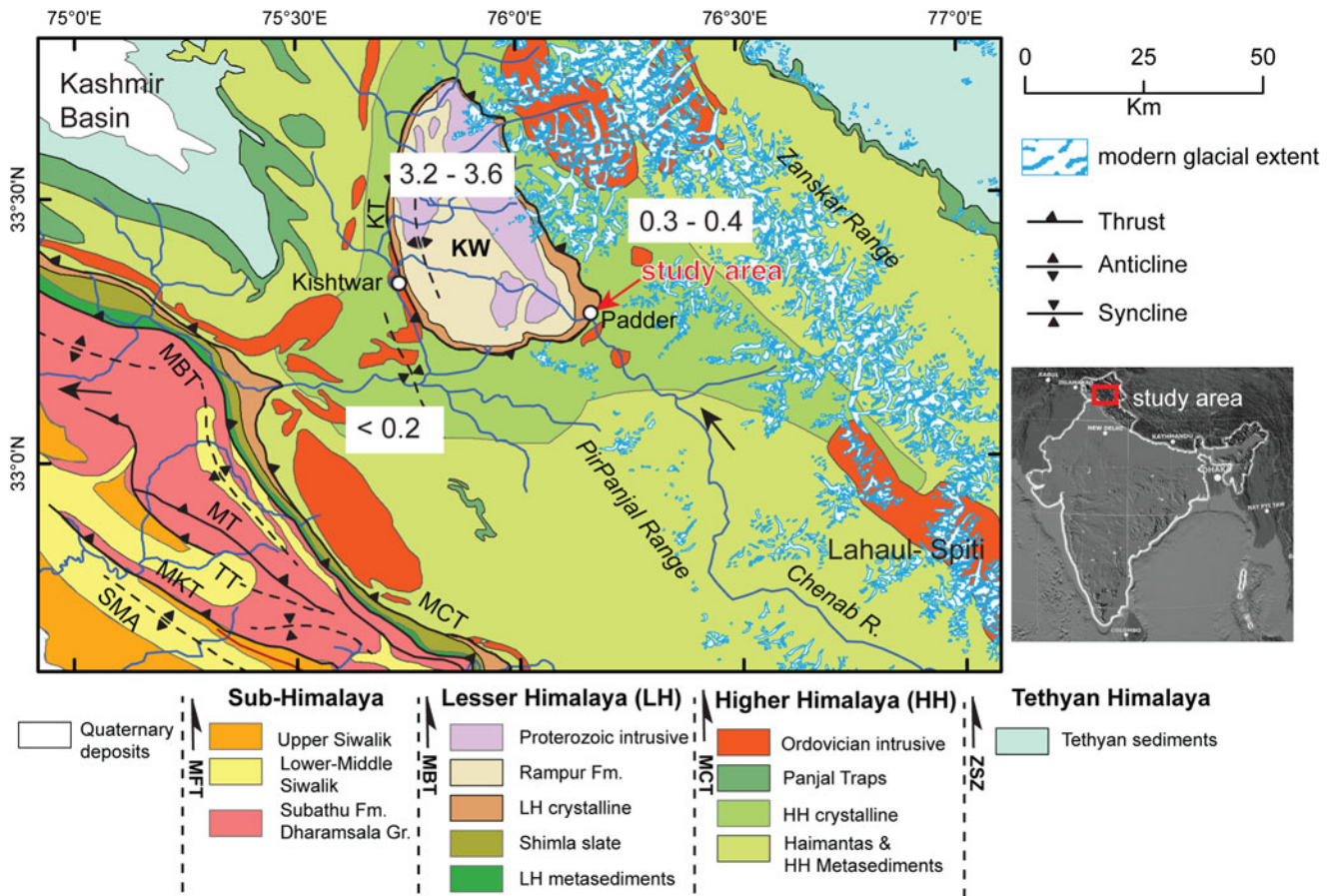
Figure 2. An overview geological map of the far-western Himalaya showing the regional lithology (modified after Steck, 2003, and Gavillot et al., 2018) and glacial extent from the GLIMS (global ice measurements from space) global database (GLIMS Consortium, 2005 [updated 2018], https://doi.org/10.7265/N5V98602; see Raup et al., 2007). Our study location is near the town of Padder, at the southeastern margin of the Kishtwar Window (KW). Note that the present-day glaciers are mostly nestled in the Higher Himalayan domain. Glacial coverage in the Higher Himalaya was more extensive during the LGM. Numbers in the white rectangles denote Quaternary exhumation rates (in mm/y) (adapted from Gavillot et al., 2018).

Clast counts were performed in the conglomeratic units of each package. For this, we used the grid method. We selected multiple 2m × 2m spots in the sediment archive and counted clasts that were >15 cm in diameter. The size filtering allowed us to count only the boulders and to cross-check our clast count by analysis of scaled photos taken in the field. Higher Himalayan (HH) and Lesser Himalayan (LH) clasts can be distinguished by their color—the Higher Himalayan clasts are darker and the granitic and quarzitic Lesser Himalayan clasts are whiter. We counted at least 250 clasts from each package and report the HH: LH clast ratio as pie charts (Fig. 4a).

The valley-fill sediments are re-incised by the Chenab River, which has sculpted at least five terrace levels in the valley (Fig. 5). We classified the terraces (T1–T5) according to their decreasing heights from the river. At present, the river still incises the valley-fill sediments in the study area. Terrace T5, lying close to the river, has a ~3–4 m thick cover of very well-sorted, well-rounded fine-grained sand. The sand layer lacks lamination.

In addition to clast counts in the field, we also determined the median size of clasts in the boulder and pebble layers from each sedimentary package (Fig. 7a) and the shape of the clasts using the commonly used axis ratios (a/b axis ratio) (Fig. 7c). From field photographs, we estimated the matrix to clast ratio by

comparing exposed surface area covered by clasts in the 2m × 2m grid used for clast count.

Luminescence dating of terrace sediments

Optically stimulated luminescence (OSL) dating is a widely accepted method for assessment of sediment depositional ages across various depositional environments and has been successfully applied to Himalayan sediments despite its low sensitivity and tendency of heterogeneous bleaching (e.g., Fuchs and Owen, 2008; Srivastava et al., 2013; Dey et al., 2021). To obtain the timing of deposition of sediments in Padder valley, we took seven samples from the medium-grained sand layers (SD/P01-P05 and SD/P07- P08) in terraces T1–T4 and one sample from the fine-grained sand layer in terrace T5 (SD/P06) for OSL measurement (Fig. 5).

OSL samples were collected in GI pipes that were 9" long. Two inches from either end of the pipe were used for dose rate measurement and the rest of the samples were chemically treated for quartz extraction. Quartz grains of 90–150 µm size fraction from the samples were extracted using standard separation protocol (Aitken, 1998) in the Physical Research Laboratory, Ahmedabad. Twenty-four aliquots of each sample were measured using a Risø TL-OSL reader in the Physical Research Laboratory,
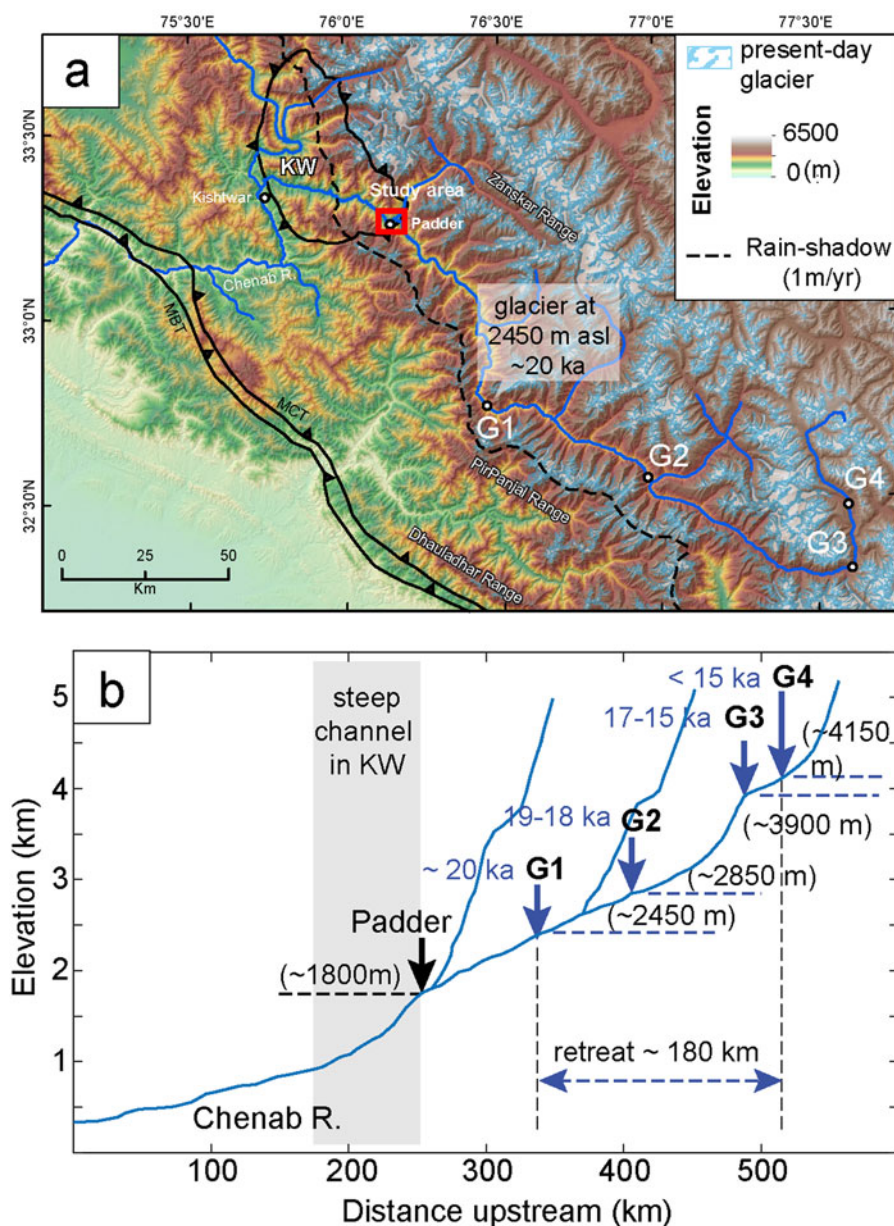
Figure 3. (**a**) Topographic map of the western Himalaya showing the glaciated landscape of the HH domain. The glacial extent (G1–G4) during and after LGM are plotted after Eugster et al., 2016. (**b**) Longitudinal profile of the Chenab River traversing the western Himalaya. Note that the Chenab valley records ~180 km retreat within a span of ca. 5 ka. Our study area lies at ~1800 m asl.

Ahmedabad. The Equivalent dose (De) for each sample was measured using the OSL Double SAR (Single Aliquot Regenerative) protocol (Roberts, 2007). Test doses were set in the range of 25–120 Gy. The aliquots were considered for ED estimation only if: (1) recycling ratio was within 1 ± 0.1, (2) De error was <20%, (3) test dose error was <10%, and (4) recuperation was below 5% of the natural. Because all the samples show over dispersion values <20%, we used the Central Age Model (CAM) to estimate De (Bailey and Arnold, 2006). Mean De $\pm 1\sigma$ for each of the samples is reported in Table 1 and Figure 8.

The dose rate was estimated using online software DRAC (Durcan et al., 2015) from the concentrations of Uranium (U), Thorium (Th), and Potassium (^{40}K) (Table 1). Thick source ZnS (Ag) alpha counter was used for determining the elemental concentrations of Uranium and Thorium, while the Potassium concentrations were estimated using NaI (Tl) gamma ray spectrometry. Estimation of moisture content was done using the fractional difference of saturated versus unsaturated sample weight and rounded off to the nearest integer (Table 1).

Sr-Nd isotopic ratios

Eleven samples were collected from the silt-clay layers in the Qp1–Qp5 sediment packages. Samples were dissolved using the standard HF-HNO$_3$-HCl dissolution protocol for silicates. Pure elemental Sr and Nd were separated from sample solutions by means of conventional cation exchange liquid chromatography with AG® 50W-X8 and Ln-spec resins from Biorad and Eichrom®, respectively, and using dilute HCl as elutants. Sr was further purified using Sr-spec resin from Eichrom® with water
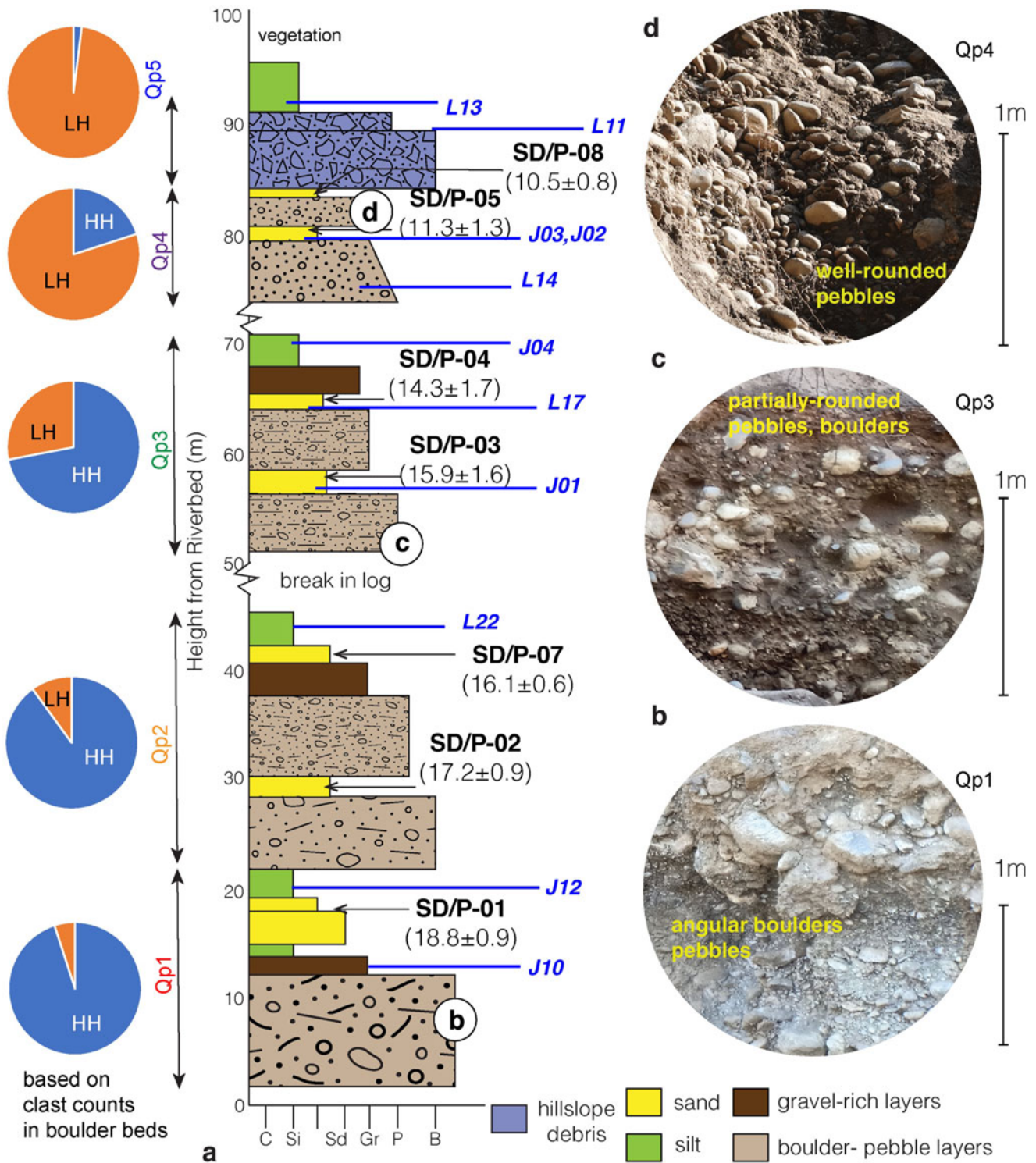
Figure 4. (**a**) Composite sediment log of the aggradation record in Upper Chenab Valley. We identified at least five fining-upward sediment packages (Qp1–Qp5) and identified those as different sediment pulses. Note the change in clast composition from Qp1 to Qp5 as the Lesser Himalayan component dominates the latter stages. (**b–d**) We also observed change in clast roundness, clast size, and matrix content of the coarsest layer of each package. Horizons labeled L and J represent samples used for statistical analysis of grain size (Fig. 7), grain shape (Fig. 7), and isotope fingerprinting (Fig. 9).

as elutant. Details of these experimental procedures are given in Chatterjee and Ray (2017, 2018). $^{87}Sr/^{86}Sr$ and $^{143}Nd/^{144}Nd$ were measured on a Thermo Fisher make Triton Plus TIMS in a multi-collection (static) mode and were corrected for machine-induced mass fractionation using $^{86}Sr/^{88}Sr$ ratio of

0.1194 and $^{146}Nd/^{144}Nd$ ratio of 0.7219, respectively. The precision values of $^{87}Sr/^{86}Sr$ and $^{143}Nd/^{144}Nd$ analyses, based on measurements of international standards NBS-987 for Sr and JNdi-1 for Nd were ± 0.000005 (2σ) and ± 0.000003 (2σ), respectively (Sr-Nd isotope ratios are listed in Table 2 and data are given in
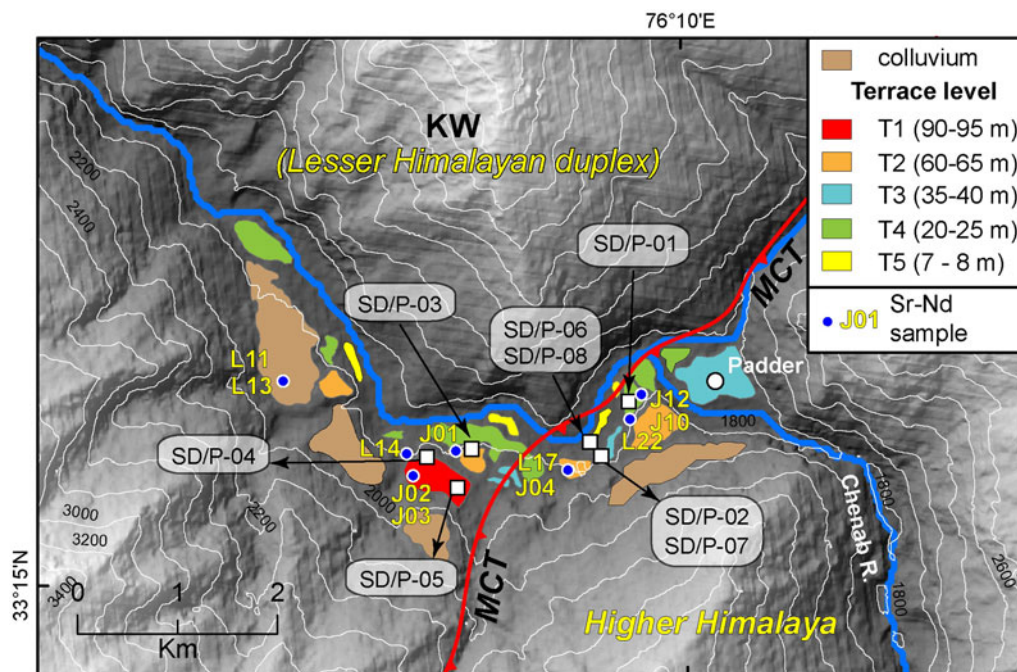
Figure 5. Topographic map of the study area showing different level of fluvial terraces, OSL and isotope sample locations near the confluence of the Chenab River and the tributary, the Padder River.

Fig. 9a). Additional analytical information is provided in Singh et al. (2022) and in the footnote of Table 2.

RESULTS

OSL chronology of terrace sediments

OSL dates of the samples SD/P-01, SD/P-02, and SD/P-07, taken from the base of the valley-fill deposits (Qp1 and Qp2), yield depositional ages of 18.8 ± 0.9 ka, 17.2 ± 0.9 ka, and 16.1 ± 0.6 ka, respectively (Table 1). Samples SD/P-03 and SD/P-04, taken from the middle of the valley-fill sediments (Qp3), give depositional ages of 15.9 ± 1.6 ka and 14.3 ± 1.7 ka, respectively. Samples SD/P-05 and SD/P-08 taken near the top of the valley-fill sediments (Qp4) provide depositional ages of 11.3 ± 1.3 ka and 10.5 ± 0.8 ka, respectively. Sample SD/P-06 from the fine-grained sand layer exposed in terrace T5, near the riverbed, produced a depositional age of 2.6 ± 0.2 ka.

Clast counts in coarser fractions

Clast counts in the field from the conglomeratic layers show a decreasing HH contribution from the bottom to the top of the sediment log (Fig. 4a). The change in HH:LH ratio in Qp1 to Qp3 is gradual, whereas the HH contribution in Qp1 is ~95%, the HH contribution in Qp2 and Qp3 is ~88% and ~70%, respectively. However, in Qp4 and Qp5, the HH fractions are unexpectedly low—only ~21% in Qp4 and almost negligible (3%) in Qp5.

Clast shape and size analysis

Clasts in the bottom parts of the sequences Qp1 and Qp2 are larger (D_{50}, the median grain-size in boulder beds, is 25–30 cm, and in pebble layers is 4.5–5.5 cm) than those in Qp3 (D_{50} in boulder beds is ~18 cm and in pebble layers is 3.6 cm) (Fig. 7). In the upper part of the archive, D_{50} values in boulder beds and pebble beds of Qp4 and Qp5 are 21–26 cm and 4–5 cm, respectively. The axis ratio of clasts is lower in both size fractions in Qp1 and Qp5 (0.4–0.5) compared to that in the middle of the section (0.8–0.9) (Fig. 7).

Isotopic fingerprinting of terrace sediments

The Sr isotopic ratio of the samples shows a narrow range of variation, $^{87}Sr/^{86}Sr = 0.757–0.810$, whereas the Nd isotopic ratios show a larger variation ($\epsilon_{Nd} = -27.2$ to -14.7; Table 2). ϵ_{Nd} values of the stratigraphically lower units are higher (-16.6 to -14.7) compared to those of the upper units (-27.2 to -21.8) (Fig. 9a).

DISCUSSION

We compiled our field, sedimentological, geochronological, and isotopic data for aggraded sediments in the Padder valley. We then compared our results with previously published records of glacial dynamics in the upper Chenab valley and global climate records to assess the role of deglaciation and monsoon intensity in the sediment aggradation observed in this part of the Himalaya.

Evolution of fluvial terraces in the Padder valley

The Padder valley records major aggradation during 20–10 ka (Table 1). The fining-upward sediment sequences (Qp1–Qp3) show sub-angular to sub-rounded clasts and poor imbrication and are identified as fluvially transported glacial outwash deposits (e.g., Maizels, 2002). The deposits are constrained within a narrow valley and are laterally continuous, therefore, arguably not related to a braided channel. Therefore, each of the sediment packages can be considered as one major pulse of a sediment-transfer event. Isolated sand layers from Qp1– Qp3 show depositional
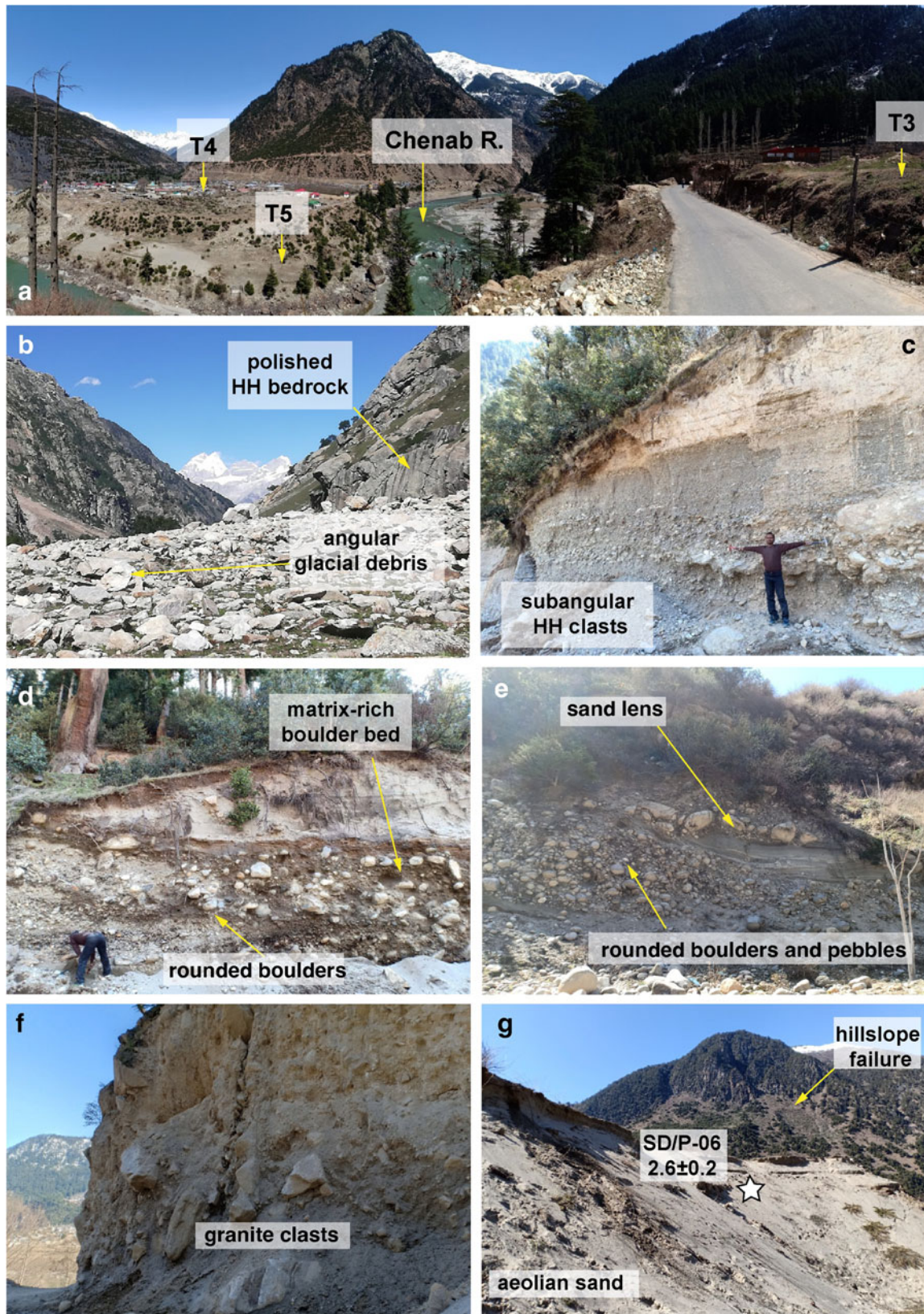
Figure 6. Field photographs. (**a**) Panoramic view of the lower terraces exposed near Padder. (**b**) Exposed glacial valley in the upper stretches of the Padder River. Angular glacial debris (HH crystalline rocks) are lying on the valley floor. (**c**) Glacial outwash sediments (Qp1) exposed in the study area showing a fining-upward sequence. (**d**) Photograph from Qp3 sediment sequence showing rounding of clasts and increase in matrix proportions. (**e**) Fluvial sequence from Qp4 showing clast-rich conglomeratic beds and isolated sand lenses. (**f**) Hillslope debris flow/landslide deposits of Qp5 only show the Lesser Himalayan granitic clasts. (**g**) T5 terrace exposing well-sorted aeolian sand.

Table 1. Details of OSL samples from Chenab valley and age calculation following a Central Age Model (after Bailey and Arnold, 2006).

Sample	Latitude (°)	Longitude (°)	U (ppm)	Th (ppm)	K (%)	H₂O (%)	Dose rate (Gy/ky)	Paleo-dose (Gy)	OD (%)	Central Age (ky)
SD/P01	33.26515	76.16135	2.9	21	2.4	6	4.43 ± 0.2	83 ± 3	10.1	18.8 ± 0.9
SD/P02	33.26198	76.15896	3.3	13.8	2.1	8	3.78 ± 0.1	65 ± 3	11.6	17.2 ± 0.9
SD/P03	33.26187	76.13881	2.8	9.5	2.6	6	3.76 ± 0.1	60 ± 6	19.2	15.9 ± 1.6
SD/P04	33.26141	76.13258	3.5	12.9	2	6	3.5 ± 0.1	50 ± 6	20.4	14.3 ± 1.7
SD/P05	33.26035	76.13083	3.9	7.2	1.9	9	3.18 ± 0.1	36 ± 4	14.5	11.3 ± 1.3
SD/P06	33.26242	76.13725	3.3	15.5	2.5	10	4.26 ± 0.1	11 ± 1	6.2	2.6 ± 0.2
SD/P07	33.26198	76.15897				10	3.85 ± 0.1	62 ± 3	16.5	16.1 ± 0.6
SD/P08	33.26243	76.13724				10	4.1 ± 0.1	43 ± 4	19.8	10.5 ± 0.8

ages varying between ca. 20–14 ka (Fig. 4a; Table 1). On the contrary, nicely rounded, polished, imbricated pebbles and cross-bedded sand bodies in Qp4 appear to be exclusively fluvial. In Qp4, the depositional ages range from ca. 11–10 ka. Qp5 is dominated by angular, disoriented granitic clasts of LH origin and is topped by a layer of fine silt. Qp5 is identified as a hillslope debris-flow deposit. Similar debris-flow deposits have been reported from the western margin of the KW (Dey et al., 2021). Qp5 is younger than 10 ka.

Clast counts in coarse fractions of the sediment archive hint at variable proportions of sediment sourcing from the HH and LH domains. The LH contribution is higher in the upper part of the archive. Isotopic source fingerprinting using $^{87}Sr/^{86}Sr$ and ϵ_{Nd} in the silt fractions of the archive also suggests the same. A simple binary mixing model involving the Higher Himalayan sequences (HH) and the Lesser Himalayan sequences (LH) as two source endmembers (Fig. 9a) clearly suggests that the silt fractions in all sampled terrace sediments of the Chenab in the Padder valley were exclusively sourced from these two Himalayan domains. Model calculations also reveal

that the (silt) sediment contribution from the HH to the valley decreased almost linearly with time since the LGM (ca. 20 ka; Fig. 9b).

Role of deglaciation in the sediment record

Glacial-interglacial cycles are linked to global solar insolation trends (e.g., Prell and Kutzbach, 1987; Huybers, 2006). Figure 1 shows low solar insolation during ca. 28–16 ka, which is known globally as the last glacial maximum (LGM). Eugster et al. (2016) estimated the LGM glacial extent along the upper Chenab valley with surface-exposure dating of glacially polished bedrocks using ^{10}Be. That study argued that at ca. 20 ka, the Chenab valley glacier had advanced down to

Table 2. Sr-Nd isotopic data for the Upper Chenab valley sediment samples.

Sample	$^{87}Sr/^{86}Sr$	$^{143}Nd/^{144}Nd$	$\epsilon_{Nd}(0)$
J-01	0.76696	0.511797	−16.4
J-02	0.76432	0.511521	−21.8
J-03	0.76852	0.511493	−22.3
J-04	0.78150	0.511641	−19.4
J-10	0.75665	0.511882	−14.7
J-12	0.76786	0.511838	−15.6
L-11	0.81019	0.511246	−27.2
L-13	0.79121	0.511434	−23.5
L-14	0.75877	0.511455	−23.1
L-17	0.77175	0.511785	−16.6
L-22	0.78521	0.511803	−16.3

Note: Sr and Nd isotope ratios were corrected for mass fractionation using $^{86}Sr/^{88}Sr = 0.1194$ and $^{146}Nd/^{144}Nd = 0.7219$, respectively. The long-term (n = 40) average values for NBS987 and JNdi-1 are $^{87}Sr/^{86}Sr = 0.710250 ± 0.000008$ and $^{143}Nd/^{144}Nd = 0.512101 ± 0.000004$ (±0.1 in ϵ_{Nd} units), respectively, at the 2σ level of uncertainty. The rock standard BHVO-2 analyzed along with the samples yielded the following values: $^{87}Sr/^{86}Sr = 0.70348$ and $^{143}Nd/^{144}Nd = 0.512968$. $\epsilon_{Nd}(0) = [(^{143}Nd/^{144}Nd)_{sample}/(^{143}Nd/^{144}Nd)_{chondrite} − 1] × 10^4$

Figure 7. Graphs showing changes in (**a**) median grain size, (**b**) matrix:clast ratio, and (**c**) axis ratios representing clast roundness from sediment packages Qp1–Qp5.

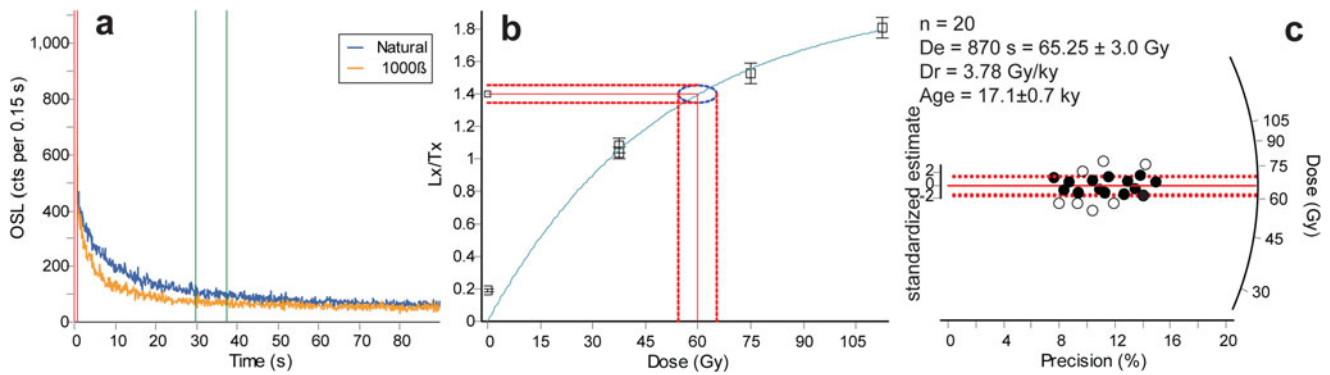**Figure 8.** (**a**) Shine curve, (**b**) dose growth curve, and (**c**) radial plot for De estimation for sample SD/P-02. Note that the black circles represent the aliquots used for the mean ± standard deviation estimation of De; n represents the total number of aliquots that passed the filter criteria described in the methods section.

~2450 m amsl and was located only ~90 km upstream from the Padder valley (see point G1 in Fig. 3), and that during the next 5–6 kyr, the glacier had retreated ~180 km to reach ~4150 m amsl (see point G4 in Fig. 3b). Similar glacial retreats likely occurred in the northern tributaries originating from the arid Zanskar Range.

Sediment chronology in the Padder valley is synchronous with the published ages of glacial retreat post-LGM. Clast counts (Fig. 4a) and isotopic compositions (Fig. 9) confirm that the sediments (Qp1–Qp3) were primarily sourced from the HH domain from 20 ka until at least 14 ka. Decreasing clast-size, increasing grain roundness and matrix to clast ratio, and decreasing HH fraction from Qp1 to Qp3 hint at longer fluvial transport for the glacial outwash sediment with time. Decreasing fraction of the HH contribution probably was a result of increasing distance from the source to the sink. The field findings and analytical results nicely corroborate the published glacial retreat history of the Chenab valley glacier (Eugster et al., 2016). Moreover, the monsoon pressure index in the Indian Ocean and simulated total precipitation in the Himalaya during 20–14 ka were lower than that of the present day (Prell and Kutzbach, 1987; Dortch et al., 2009), which in turn suggests that the ISM had little control over the formation of Qp1–Qp3. Therefore, we relate the majority of sediment aggradation (~70 m) to deglaciation in the upper Chenab valley or southern flank of the Zanskar Range, located to the north of the Padder valley.

Effect of monsoon cycle on sediment aggradation and re-incision

The HH domain hosts the majority of the glaciers, therefore, it is expected to be affected by deglaciation more than the LH domain. It is generally thought that major deglaciation in the Himalaya had ceased by 14 ka and the extent of glaciation has remained almost unchanged since then (Eugster et al., 2016; Fig. 3a). As mentioned earlier, Qp4 (11–10 ka) has a prominent fluvial signature and has ~80% contribution from the LH in the pebble-boulder fraction (Fig. 4a) and 30–40% in the silt fraction (Fig. 9b). Therefore, Qp4 has more contribution from the LH domain, which didn't have glacial coverage post-LGM. Slight decrease in roundness and increase in clast size in comparison to Qp3, further suggest shorter transport for Qp4 sediment. Thus, Qp4 has a lower HH or glacial source, having sediments that originated from the non-glaciated hillslopes of the

surrounding LH. The Early Holocene (12–8 ka) was characterized by strong monsoon, with monsoon pressure index up to 40% higher and the total simulated precipitation 10% higher than the present day (Prell and Kutzbach, 1987; Dortch et al., 2009; Gebregiorgis et al., 2016). Many of the western Himalayan valleys exhibit aggradation during this period (e.g., Bookhagen et al., 2006; Srivastava et al., 2008; Dey et al., 2016). Therefore, aggradation of Qp4 can be attributed to the Early Holocene (12–10 ka) intensified ISM.

An almost linear decrease in the HH contribution in the sediment signal with time (Fig. 9b) points to two possible scenarios. (1) Increasing distance from the sediment source—The Higher Himalayan glaciers were the major source of sediments during the entire aggradation phase (Qp1–Qp4). However, as the glaciers retreated upstream, the source to sink distance became >300 km by the Early Holocene. Higher HH contribution in the silt fraction versus in the clast fraction supports the claim of longer fluvial transport of the HH-derived sediment. (2) Shift in erosional domain—The steeper hillslopes of the HH domain would have aided enhanced erosion due to a stronger monsoon. However, in a recently published study from the Dhauladhar region in western Himalaya, Dey et al. (2021) have shown that the moderately steep regions are more sensitive to climate change and, therefore, the response to change in monsoon intensity was higher in the LH domain. That is why in Qp4, the abundance of HH clasts is lower (60–70%) than that in Qp1–Qp3 (>80%) (Fig. 7b).

Since 8–10 ka, the Padder valley experienced recurring re-incision of transiently stored sediment. Each re-incision phase was marked by formation of fluvial-fill terraces (T1–T4). Holocene staircase terraces are common in the Himalayan valleys across wet to semi-arid landscapes (e.g., Pratt-Sitaula et al., 2004; Bookhagen et al., 2006; Sinha et al., 2010; Dutta et al., 2012, 2018; Dey et al., 2016; Chahal et al., 2019). Barring a few instances (e.g., Sinha et al., 2010; Dutta et al., 2012), episodic weakening of the ISM has been linked to the formation of these Holocene terraces. Thus, the Padder valley morphology appears to attest to a synchronized Holocene sediment removal from the Himalayan valleys.

Debris flows and landslides during the Early Holocene

Landslides triggered by earthquakes are as common as rainfall-driven landslides in the High mountains (e.g., Bookhagen et al., 2005a, b; Parkash, 2013). Landslides and hillslope debris flows
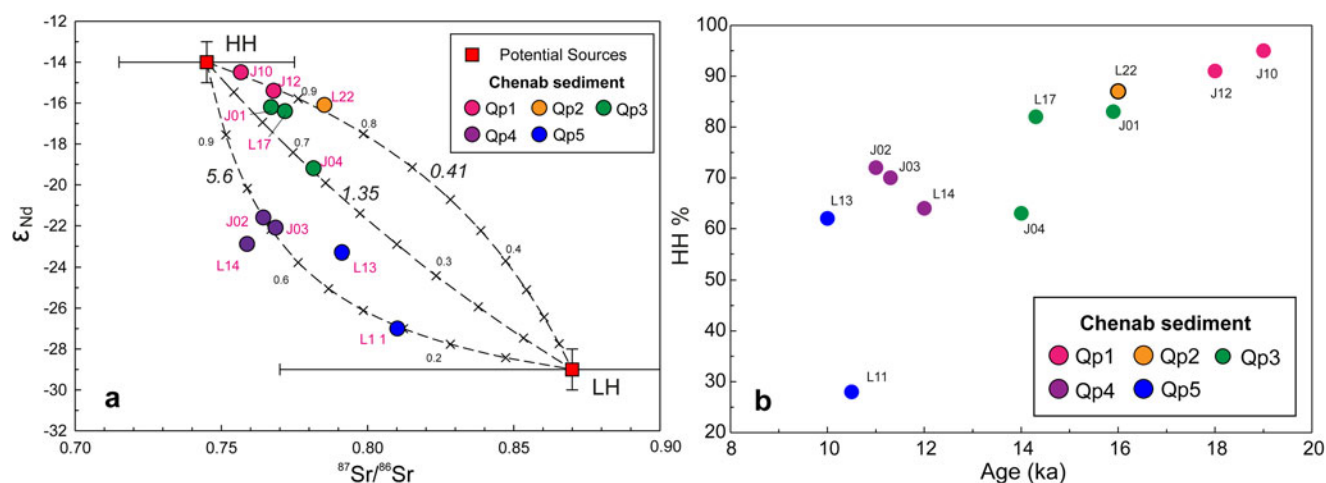
Figure 9. (**a**) Plot of ϵ_{Nd} versus $^{87}Sr/^{86}Sr$ for sediment samples (labeled) from the Chenab River Valley terraces near Padder, Jammu & Kashmir. The data are compared with the average isotopic compositions (± 1σ) of rocks of the Higher Himalayan (HH) sequences and the Lesser Himalaya (LH) sequences of the region, which are the potential sediment sources for the Chenab River (data sources: Miller et al., 2000, 2001). The dashed lines are binary mixing curves between the two source endmembers, with fraction of the HH in the mixture marked. The italicized number on each curve is $(Sr_A/Sr_B)/(Nd_A/Nd_B)$, where A and B stand for HH and LH, respectively. (**b**) Plot showing decreasing HH contribution with time.

that define the Qp5 aggradation sequence occurred in the Early Holocene. Clast counts and valley morphology confirm that the source of sediments in Qp5 is the valley walls of the surrounding LH domain. Negligible HH contribution in the clast fraction and much-reduced HH component in the silt fraction (Fig. 9) could possibly indicate reworking and incorporation of Qp4 sediments into the mass flow. The Early Holocene period is characterized by a strong ISM. Increased monsoon strength could have activated the meta-stable hillslopes of the eastern edge of the KW. Seismic epicenter maps of this region (Supplementary Fig. S3) show considerable numbers of small- to moderate-magnitude earthquakes (Mw: 3–5) in this region, suggesting possible occurrences of similar activity in the past as well. Penecontemporaneous deformation structures in soft sediments are common features in the Himalayan sediment archives affected by concurrent seismicity (e.g., Kotlia and Rawat, 2004; Phartiyal and Sharma, 2009; Mugnier et al., 2011). Absence of penecontemporaneous deformation structures in the studied sediment sequences doesn't confirm the role of seismicity; however, we are not able to completely rule out its possibility. Similar conclusions were drawn by Dortch et al. (2009) where they studied large landslides in the Himalaya. To add to this, decadal- to centennial-scale seismic data cannot be extrapolated up to 20 ky ago when the deposition initiated. Therefore, the role of tectonics cannot be verified with the available data.

Large-scale seismic activity in the Himalaya could be responsible for the formation of landslide-dammed lakes (e.g., Korup et al., 2010; Kumar et al., 2021). However, there are no lacustrine deposits stored at the base of the aggradation sequence in the Padder valley. Lacustrine deposits could well have been completely incised by the river or buried by the aeolian sediments near the present-day stream. Not finding a lacustrine deposit certainly doesn't mean that it was not there. However, because we could not find any evidence, the role of landslide-damming cannot be evaluated with the available dataset and field findings. We have observed several modern-day landslides/hillslope failures in the eastern fringes of the KW; however, they are much smaller in size and probably are incapable of blocking the Chenab River.

Role of aridity during the Late Holocene

The lowest terrace (T5) records a ~4 m thick fine-grained sand capping (Fig. 5f). The sand capping is devoid of any recognizable laminations, the grain-size is small (80 ± 20 µm) and sorting is high. A single depositional age from this aeolian sand layer suggests a Late Holocene age (age-SD/P-06: 2.6 ± 0.1 ka). The De estimates of sample SD/P-06 form a cluster resulting a low over-dispersion value (OD ~6%; Table 1), which suggests that the sample was uniformly (well) bleached. We interpret the sand layer as a loess deposit. Surface-draping aeolian deposits are common in the arid western Himalaya (e.g., Kumar et al., 2017). Based on OSL-dated moraines, Bisht et al. (2017) proposed a protracted arid phase during ca. 5–3 ka in the western Himalaya. A previous study by Khan et al. (2022) suggested the existence of a period of aridity in the Himalaya during 4–1 ka. Although we have very limited age control, the loess deposit in the Padder valley could be broadly linked with this dry phase.

CONCLUSIONS

Combining the results from our field observations and analytical results, in conjunction with inferences made by earlier studies, we reach the following conclusions. (1) Sediment aggradation in the Padder valley happened during 20–10 ka and was followed by recurring incision, leading to formation of staircase fill terraces. (2) Field evidence and analytical results neither can verify nor can rule out any tectonic trigger behind the aggradation. Rather, the observed sediment aggradation and re-incision followed the trend of global climatic fluctuations, suggesting climatic control on sediment transfer. (3) Initial stages of terrace sedimentation were dominated by fluvially transported glacial outwash sediments that bore signatures of the Higher Himalayan provenance. In contrast, the upper part of the archive exhibited reduced influence of the glaciated Higher Himalaya and contained a significant contribution from the non-glaciated Lesser Himalayan sources. Overall, glacial sediments dominate (~70%) the total sediment deposition in the valley. (4) The decrease in the Higher Himalayan contribution to the sediment archive with

time could be attributed either to retreat of the Chenab valley glacier or to increased erosion of the Lesser Himalayan domain during the Early Holocene, or a combination of both. The first is supported by the 180 km glacial retreat during 20–15 ka in the Upper Chenab valley, and the second is backed by increased erosion in the Lesser Himalayan domain.

This study highlights a dominant role of glacial dynamics on the aggradation pattern observed in a fluvial valley in the Higher Himalaya. The role of glaciers needs to be investigated further in other fluvial networks to understand the complexity of sediment transfer in response to climate change.

REFERENCES

Adams, B.A., Whipple, K.X., Forte, A.M., Heimsath, A.M., Hodges, K.V., 2020. Climate controls on erosion in tectonically active landscapes. *Science Advances* **6**, eaaz3166. https://doi.org/10.1126/sciadv.aaz3166.

Aitken, M.J., 1998. *Introduction to Optical Dating: the Dating of Quaternary Sediments by the Use of Photon-stimulated Luminescence.* Clarendon Press, Oxford, New York, Tokyo, 267 pp.

Bailey, R.M. and Arnold, L.J., 2006. Statistical modelling of single grain quartz De distributions and an assessment of procedures for estimating burial dose. *Quaternary Science Reviews* **25**, 2475–2502.

Barnard, P.L., Owen, L.A., Finkel, R.C., 2004. Style and timing of glacial and paraglacial sedimentation in a monsoon-influenced high Himalayan environment, the upper Bhagirathi Valley, Garhwal Himalaya. *Sedimentary Geology* **165**, 199–221.

Bisht, P., Ali, S.N., Rana, N., Singh, S., Sundriyal, Y.P., Bagri, D.S., Juyal, N., 2017. Pattern of Holocene glaciation in the monsoon-dominated Kosa Valley, central Himalaya, Uttarakhand, India. *Geomorphology* **284**, 130–141.

Bookhagen, B., Burbank, D.W., 2006. Topography, relief, and TRMM-derived rainfall variations along the Himalaya. *Geophysical Research Letters* **33**, L08405. https://doi.org/10.1029/2006GL026037.

Bookhagen, B., Fleitmann, D., Nishiizumi, K., Strecker, M.R., Thiede, R.C., 2006. Holocene monsoonal dynamics and fluvial terrace formation in the northwest Himalaya, India. *Geology* **34**, 601–604.

Bookhagen, B., Strecker, M.R., 2012. Spatiotemporal trends in erosion rates across a pronounced rainfall gradient: examples from the southern Central Andes. *Earth and Planetary Science Letters* **327**, 97–110.

Bookhagen, B., Thiede, R.C., Strecker, M.R., 2005a. Late Quaternary intensified monsoon phases control landscape evolution in the northwest Himalaya. *Geology* **33**, 149–152.

Bookhagen, B., Thiede, R.C., Strecker, M.R., 2005b. Abnormal monsoon years and their control on erosion and sediment flux in the high, arid northwest Himalaya. *Earth and Planetary Science Letters* **231**, 131–146.

Chahal, P., Kumar, A., Sharma, C.P., Singhal, S., Sundriyal, Y.P., Srivastava, P., 2019. Late Pleistocene history of aggradation and incision, provenance and channel connectivity of the Zanskar River, NW Himalaya. *Global and Planetary Change* **178**, 110–128.

Chatterjee, A., Ray, J.S., 2017. Sources and depositional pathways of mid-Holocene sediments in the Great Rann of Kachchh, India: implications for fluvial scenario during the Harappan Culture. *Quaternary International* **443**, 177–187.

Chatterjee, A., Ray, J.S., 2018. Geochemistry of Harappan potteries from Kalibangan and sediments in the Ghaggar River: clues for a dying river. *Geoscience Frontiers* **9**, 1203–1211.

Clift, P.D., 2017. Cenozoic sedimentary records of climate-tectonic coupling in the Western Himalaya. *Progress in Earth and Planetary Science* **4**, 39. https://doi.org/10.1186/s40645-017-0151-8.

Clift, P.D., Giosan, L., Blusztajn, J., Campbell, I.H., Allen, C., Pringle, M., Tabrez, A.R., et al., 2008. Holocene erosion of the Lesser Himalaya triggered by intensified summer monsoon. *Geology* **36**, 79–82.

Dadson, S.J., Hovius, N., Chen, H., Dade, W.B., Lin, J.C., Hsu, M.L., Lin, C.W., et al., 2004. Earthquake-triggered increase in sediment delivery from an active mountain belt. *Geology* **32**, 733–736.

Dey, S., Bookhagen, B., Thiede, R.C., Wittmann, H., Chauhan, N., Jain, V., Strecker, M.R., 2022. Impact of Late Pleistocene climate variability on paleo-erosion rates in the western Himalaya. *Earth and Planetary Science Letters* **578**, 117326. https://doi.org/10.1016/j.epsl.2021.117326.

Dey, S., Thiede, R. C., Biswas, A., Chauhan, N., Chakravarti, P., Jain, V., 2021. Implications of the ongoing rock uplift in NW Himalayan interiors. *Earth Surface Dynamics* **9**, 463–485.

Dey, S., Thiede, R.C., Schildgen, T.F., Wittmann, H., Bookhagen, B., Scherler, D., Jain, V., Strecker, M.R., 2016. Climate-driven sediment aggradation and incision since the Late Pleistocene in the NW Himalaya, India. *Earth and Planetary Science Letters* **449**, 321–331.

Dortch, J.M., Owen, L.A., Haneberg, W.C., Caffee, M.W., Dietsch, C., Kamp, U., 2009. Nature and timing of large landslides in the Himalaya and Transhimalaya of northern India. *Quaternary Science Reviews* **28**, 1037–1054.

Durcan, J.A., King, G.E., Duller, G.A., 2015. DRAC: Dose Rate and Age Calculator for trapped charge dating. *Quaternary Geochronology* **28**, 54–61.

Dutta, S., Mujtaba, S.A.I., Saini, H.S., Chunchekar, R., Kumar, P., 2018. Geomorphic evolution of glacier-fed Baspa Valley, NW Himalaya: record of late Quaternary climate change, monsoon dynamics and glacial fluctuations. *Geological Society, London, Special Publications* **462**, 51–72.

Dutta, S., Suresh, N., Kumar, R., 2012. Climatically controlled late Quaternary terrace staircase development in the fold-and-thrust belt of the Sub Himalaya. *Palaeogeography, Palaeoclimatology, Palaeoecology* **356**, 16–26.

Eugster, P., Scherler, D., Thiede, R.C., Codilean, A.T., Strecker, M.R., 2016. Rapid last glacial maximum deglaciation in the Indian Himalaya coeval with midlatitude glaciers: new insights from [10]Be-dating of ice-polished bedrock surfaces in the Chandra Valley, NW Himalaya. *Geophysical Research Letters* **43**, 1589–1597.

Fuchs, M., Owen, L. A., 2008. Luminescence dating of glacial and associated sediments: review, recommendations and future directions. *Boreas* **37**, 636–659.

Gavillot, Y., Meigs, A.J., Sousa, F.J., Stockli, D., Yule, D., Malik, M., 2018. Late Cenozoic foreland-to-hinterland low-temperature exhumation history of the Kashmir Himalaya. *Tectonics* **37**, 3041–3068.

Gebregiorgis, D., Hathorne, E.C., Sijinkumar, A.V., Nath, B.N., Nürnberg, D., Frank, M., 2016. South Asian summer monsoon variability during the last ~54 kas inferred from surface water salinity and river runoff proxies. *Quaternary Science Reviews* **138**, 6–15.

Gibling, M.R., Tandon, S.K., Sinha, R., Jain, M., 2005. Discontinuity-bounded alluvial sequences of the southern Gangetic Plains, India: aggradation and degradation in response to monsoonal strength. *Journal of Sedimentary Research* **75**, 369–385.

GLIMS Consortium, 2005 [updated 2018]. *GLIMS Glacier Database, Version 1.* Distributed by NASA National Snow and Ice Data Center Distributed Active Archive Center. https://doi.org/10.7265/N5V98602. Date accessed February 4, 2021.

Godard, V., Bourlès, D.L., Spinabella, F., Burbank, D.W., Bookhagen, B., Fisher, G.B., Moulin, A., Léanni, L., 2014. Dominance of tectonics over climate in Himalayan denudation. *Geology* **42**, 243–246.

Goodbred, S.L., Jr., Kuehl, S.A., 2000. Enormous Ganges-Brahmaputra sediment discharge during strengthened early Holocene monsoon. *Geology* **28**, 1083–1086.

Huybers, P., 2006. Early Pleistocene glacial cycles and the integrated summer insolation forcing. *Science* **313**, 508–511.

International Seismological Centre, 2021. ISC-GEM Earthquake Catalogue. https://doi.org/10.31905/d808b825. Date accessed February 4, 2021.

Joussain, R., Colin, C., Liu, Z., Meynadier, L., Fournier, L., Fauquembergue, K., Zaragosi, S., Schmidt, F., Rojas, V., Bassinot, F., 2016. Climatic control of sediment transport from the Himalayas to the

proximal NE Bengal Fan during the last glacial-interglacial cycle. *Quaternary Science Reviews* **148**, 1–16.

Kapannusch, R., Scherler, D., King, G., Wittmann, H., 2020. Glacial influence on Late Pleistocene [10]Be-derived paleo-erosion rates in the northwestern Himalaya, India. *Earth and Planetary Science Letters* **547**, 116441. https://doi.org/10.1016/j.epsl.2020.116441.

Khan, F., Meena, N.K., Sundriyal, Y., Sharma, R., 2022. Indian summer monsoon variability during the last 20 kyr: evidence from peat record from the Baspa Valley, northwest Himalaya, India. *Journal of Earth System Science* **131**, 164. https://doi.org/10.1007/s12040-022-01906-0.

Korup, O., Montgomery, D.R., Hewitt, K., 2010. Glacier and landslide feedbacks to topographic relief in the Himalayan syntaxes. *Proceedings of the National Academy of Sciences* **107**, 5317–5322.

Kotlia, B.S., Rawat, K.S., 2004. Soft sediment deformation structures in the Garbyang palaeolake: evidence for the past shaking events in the Kumaun Tethys Himalaya. *Current Science-Bangalore* **87**, 377–379.

Kulkarni, A.V., Bahuguna, I.M., Rathore, B.P., Singh, S.K., Randhawa, S.S., Sood, R.K., Dhar, S., 2007. Glacial retreat in Himalaya using Indian remote sensing satellite data. *Current Science* **92**, 69–74.

Kumar, A., Srivastava, P., Meena, N. K., 2017. Late Pleistocene aeolian activity in the cold desert of Ladakh: a record from sand ramps. *Quaternary International* **443**, 13–28.

Kumar, V., Jamir, I., Gupta, V., Bhasin, R. K., 2021. Inferring potential landslide damming using slope stability, geomorphic constraints, and run-out analysis: a case study from the NW Himalaya. *Earth Surface Dynamics* **9**, 351–377.

Lane, E.W., 1955. The importance of fluvial morphology in hydraulics. *Proceedings of the American Society of Civil Engineers* **81**(7), 1–17.

Maizels, J., 2002. Sediments and landforms of modern proglacial terrestrial environments. In: Menzies, J. (Ed.), *Modern and Past Glacial Environments*. Butterworth-Heinemann, Oxford, pp. 279–316.

Mandal, S.K., Scherler, D., Wittmann, H., 2021. Tectonic accretion controls erosional cyclicity in the Himalaya. *AGU Advances* **2**, e2021AV000487. https://doi.org/10.1029/2021AV000487.

Miller, C., Klötzli, U., Frank, W., Thöni, M., Grasemann, B., 2000. Proterozoic crustal evolution in the NW Himalaya (India) as recorded by circa 1.80 Ga mafic and 1.84 Ga granitic magmatism. *Precambrian Research* **103**, 191–206.

Miller, C., Thöni, M., Frank, W., Grasemann, B., Klötzli, U., Guntli, P., Draganits, E., 2001. The early Palaeozoic magmatic event in the Northwest Himalaya, India: source, tectonic setting and age of emplacement. *Geological Magazine* **138**, 237–251.

Mugnier, J.L., Huyghe, P., Gajurel, A.P., Upreti, B.N., Jouanne, F., 2011. Seismites in the Kathmandu Basin and seismic hazard in central Himalaya. *Tectonophysics* **509**, 33–49.

Owen, L.A., Finkel, R.C., Caffee, M.W., 2002. A note on the extent of glaciation throughout the Himalaya during the global last glacial maximum. *Quaternary Science Reviews* **21**, 147–157.

Parkash, S., 2013. Earthquake related landslides in the Indian Himalaya: experiences from the past and implications for the future. In: Margottini, C., Canuti, P., Sassa, K. (Eds.), *Landslide Science and Practice*. Springer, Berlin, Heidelberg, pp. 327–334.

Phartiyal, B., Sharma, A., 2009. Soft-sediment deformation structures in the late Quaternary sediments of Ladakh: evidence for multiple phases of seismic tremors in the north western Himalayan Region. *Journal of Asian Earth Sciences* **34**, 761–770.

Pratt-Sitaula, B., Burbank, D.W., Heimsath, A., Ojha, T., 2004. Landscape disequilibrium on 1000–10,000 year scales Marsyandi River, Nepal, central Himalaya. *Geomorphology* **58**, 223–241.

Prell, W.L., Kutzbach, J.E., 1987. Monsoon variability over the past 150,000 years. *Journal of Geophysical Research: Atmospheres* **92**, 8411–842.

Raup, B.H., Raciviteanu, A., Khalsa, S.S., Helm, C., Armstrong, R., Arnaud, Y., 2007. The GLIMS geospatial glacier database: a new tool for studying glacier change. *Global and Planetary Change* **56**. https://doi.org/10.1016/j.gloplacha.2006.07.018.

Ray, Y., Srivastava, P., 2010. Widespread aggradation in the mountainous catchment of the Alaknanda-Ganga River system: timescales and implications to Hinterland-foreland relationships. *Quaternary Science Reviews* **29**, 2238–2260.

Roberts, H.M., 2007. Assessing the effectiveness of the double-SAR protocol in isolating a luminescence signal dominated by quartz. *Radiation Measurements* **42**, 1627–1636.

Scherler, D., Bookhagen, B., Wulf, H., Preusser, F., Strecker, M.R., 2015. Increased Late Pleistocene erosion rates during fluvial aggradation in the Garhwal Himalaya, northern India. *Earth and Planetary Science Letters* **428**, 255–266.

Singh, A.K., Parkash, B., Mohindra, R., Thomas, J.V., Singhvi, A.K., 2001. Quaternary alluvial fan sedimentation in the Dehradun Valley piggyback basin, NW Himalaya: tectonic and palaeoclimatic implications. *Basin Research* **13**, 449–471.

Singh, A., Ray, J.S., Jain, V., Mahala, M.K., 2022. Evaluating the connectivity of the Yamuna and the Sarasvati during the Holocene: evidence from geochemical provenance of sediment in the Markanda River Valley, India. *Geomorphology* **402**, 108124. https://doi.org/10.1016/j.geomorph.2022.108124.

Sinha, S., Suresh, N., Kumar, R., Dutta, S., Arora, B.R., 2010. Sedimentologic and geomorphic studies on the Quaternary alluvial fan and terrace deposits along the Ganga exit. *Quaternary International* **227**, 87–103.

Srivastava, P., Kumar, A., Mishra, A., Meena, N.K., Tripathi, J.K., Sundriyal, Y.P., Agnihotri, R., Gupta, A.K., 2013. Early Holocene monsoonal fluctuations in the Garhwal higher Himalaya as inferred from multi-proxy data from the Malari paleolake. *Quaternary Research* **80**, 447–458.

Srivastava, P., Tripathi, J.K., Islam, R., Jaiswal, M.K., 2008. Fashion and phases of Late Pleistocene aggradation and incision in the Alaknanda River Valley, western Himalaya, India. *Quaternary Research* **70**, 68–80.

Steck, A., 2003. Geology of the NW Indian Himalaya. *Eclogae Geologicae Helvetiae* **96**, 147–196.

Strecker, M.R., Alonso, R.N., Bookhagen, B., Carrapa, B., Hilley, G.E., Sobel, E.R., Trauth, M.H., 2007. Tectonics and climate of the southern central Andes. *Annual Review of Earth and Planetary Sciences* **35**, 747–787.

Suresh, N., Bagati, T.N., Kumar, R., Thakur, V.C., 2007. Evolution of Quaternary alluvial fans and terraces in the intramontane Pinjaur Dun, Sub-Himalaya, NW India: interaction between tectonics and climate change. *Sedimentology* **54**, 809–833.

Tofelde, S., Schildgen, T.F., Savi, S., Pingel, H., Wickert, A.D., Bookhagen, B., Wittmann, H., Alonso, R.N., Cottle, J., Strecker, M.R., 2017. 100 kyr fluvial cut-and-fill terrace cycles since the Middle Pleistocene in the southern Central Andes, NW Argentina. *Earth and Planetary Science Letters* **473**, 141–153.

Vannay, J.C., Grasemann, B., Rahn, M., Frank, W., Carter, A., Baudraz, V., Cosca, M., 2004. Miocene to Holocene exhumation of metamorphic crustal wedges in the NW Himalaya: evidence for tectonic extrusion coupled to fluvial erosion. *Tectonics* **23**, TC1014. https://doi.org/10.1029/2002TC001429.

Wang, W., Godard, V., Liu-Zeng, J., Scherler, D., Xu, C., Zhang, J., Xie, K., Bellier, O., Ansberque, C., de Sigoyer, J., ASTER Team, 2017. Perturbation of fluvial sediment fluxes following the 2008 Wenchuan earthquake. *Earth Surface Processes and Landforms* **42**, 2611–2622.

Whipple, K.X., 2009. The influence of climate on the tectonic evolution of mountain belts. *Nature Geoscience* **2**, 97–104.